

# Influence of Surface Chemistry on Carbon Fiber Structural Battery Anodes

Muhammad Aqeel, Bhagya Dharmasiri, Ruben Tavano, Elmer Austria, Behnam Akhavan, Leif E. Asp, Luke C. Henderson,\* and James D. Randall\*

Carbon fiber (CF) electrodes offer a promising route to enhance both mechanical and electrochemical performance in multifunctional structural batteries for future technologies such as electric vehicles, next-generation aircraft, and autonomous satellites. Recent developments have focused on solid battery electrolytes that deliver both ionic conductivity and mechanical strength. Central to this is the CF interface, which plays a dual role in structural reinforcement and charge storage. While interfacial chemistry is well studied in composites, its impact on the anode performance of CFs tailored for mechanical performance remains unclear. This article explores how CF surface chemistry influences

electrochemical battery performance, by grafting functional groups known to improve composite adhesion ( $\text{NO}_2$ ,  $\text{NH}_2$ ,  $\text{SH}$ ,  $\text{SO}_3\text{H}$ ). Surface modifications are confirmed using scanning electron microscopy, Raman spectroscopy, and X-ray photoelectron spectroscopy. Untreated CFs delivered an initial capacity of  $189.1 \pm 42.6 \text{ mAh g}^{-1}$ , while SH- and  $\text{NO}_2$ -functionalized CFs achieved enhanced capacities of  $244.0 \pm 12.1$  and  $243.8 \pm 64.1 \text{ mAh g}^{-1}$ , respectively. These results suggest that chemical surface modification—while originally intended for composite performance—may also improve the anode performance in structural battery systems.

## 1. Introduction

The growing concerns over fossil fuel consumption and its environmental impact have driven the demand for more energy-efficient technologies, particularly in the transportation industry.<sup>[1–3]</sup> Vehicles are major contributors to global emissions, and one of the most effective strategies to improve fuel efficiency and reduce emissions is through replacing material components with lightweight alternatives.<sup>[4–6]</sup> By doing so, vehicles can

achieve better energy performance and extended driving ranges, especially critical for electric vehicles.<sup>[7–9]</sup>

To further enhance energy efficiency, there is increasing interest in multifunctional materials such as structural batteries—systems that simultaneously store electrochemical energy and carry mechanical load.<sup>[10,11]</sup> Conventional lithium-ion batteries (LIBs) are solely energy storage devices and contribute significantly to system mass without offering structural support.<sup>[12,13]</sup> By embedding energy storage into structural components, structural batteries can reduce overall system weight and volume and increase driving efficiency. Recent reports by Johannesson and coworkers calculated that by replacing the roof of an electric vehicle with a structural battery, 20% mass savings could be attained while contributing additional onboard energy storage.<sup>[14,15]</sup>

Carbon fiber (CF) composites are well suited for such structural battery applications, as CFs can act simultaneously as load-bearing elements, current collectors, and as lithium-intercalating anodes,<sup>[16]</sup> while the surrounding resin matrix can serve as a solid electrolyte and/or host electroactive materials. This dual functionality allows for integration of electrochemical and mechanical performance within a single composite architecture.<sup>[17–19]</sup>

It is important to recognize that the purpose of structural battery systems are fundamentally different compared to conventional LIB. In traditional batteries, energy and power density are paramount and the materials heavily optimized for electrochemical performance. Such systems are often physically segregated from the structural frame of an EV due to lack of mechanical robustness. In contrast, load-bearing components of a typical EV can be replaced with structural batteries, accordingly, the main function of a structural battery is to be mechanically

M. Aqeel, B. Dharmasiri, L. C. Henderson, J. D. Randall  
Institute for Frontier Materials  
Deakin University  
Waurn Ponds, Victoria 3216, Australia  
E-mail: luke.henderson@deakin.edu.au  
J.Randall@deakin.edu.au

R. Tavano, L. E. Asp  
Department of Industrial and Materials Science  
Chalmers University of Technology  
41258 Göteborg, Sweden

E. Austria, B. Akhavan  
School of Biomedical Engineering  
Faculty of Engineering  
University of Sydney  
Sydney, NSW 2006, Australia

B. Akhavan  
School of Engineering  
University of Newcastle  
Callaghan, NSW 2308, Australia

B. Akhavan  
Precision Medicine Program  
Hunter Medical Research Institute (HMRI)  
New Lambton Heights, NSW 2305, Australia

 Supporting information for this article is available on the WWW under <https://doi.org/10.1002/batt.202500464>

robust whilst allowing additional energy storage and extraction functionalities. As such, anode materials that serve in structural batteries—such as CFs—should not be directly compared with state-of-the-art graphite or silicon-based anodes, which are incompatible with load-bearing applications. The end goal is to have the two battery systems operating in complementarity.

There has been extensive research on the use of CFs derived from various precursors in structural batteries, particularly as anode materials.<sup>[20,21]</sup> The specific storage capacity of CFs varies significantly depending on how it was manufactured, what charge rate is applied and what sizing's are on the fiber surface. The most common CF derived from Polyacrylonitrile (PAN) T300 and T700 fibers exhibit a specific capacity of 150 and 170 mAh g<sup>-1</sup>, respectively at a charge rate of C/10.<sup>[22]</sup> However, pitch derived fibers exhibited a specific capacity of only 10 mAh g<sup>-1</sup> at C/10. Considering that pitch-based CF is far more graphitic in its structure, this counterintuitive outcome suggesting that an amorphous and nitrogen rich graphene-like structure is preferable over a highly graphitic crystalline structure for lithiation.<sup>[23–25]</sup>

Despite the promise of CF-based structural batteries, there are several critical challenges that hinder their full potential. One major issue is that the full reinforcing potential and mechanical strength of continuous, pristine CF cannot be fully utilized when embedded in a solid polymer electrolyte (SPE) matrix. SPEs typically exhibit low mechanical strength compared to high-performance thermosets or thermoplastics,<sup>[26–28]</sup> and this mismatch often makes the use of ultrastrong, continuous CF unnecessary or even excessive in terms of material performance and cost. Additionally, the CF is typically not completely bonded to the resin as some fiber surface must be in contact with the electrolyte to allow ion conductivity. Thus, the structural benefits of pristine CF are not fully realized due to the limitations of the surrounding matrix, leading to inefficiencies in both mechanical performance and resource use.<sup>[29,30]</sup>

To address this, recycled CFs (rCFs) present a compelling alternative. These fibers are often available in discontinuous or non-woven fabric forms, making them more compatible practically, as they are self-supporting electrodes. They also align with sustainability goals by reducing manufacturing waste and carbon emissions.<sup>[31,32]</sup> From a processing perspective, rCFs offer enhanced design flexibility for integrating electrolytes and active materials into the matrix, which can further support ionic conductivity and overall battery performance.<sup>[33]</sup> Their cost-effectiveness and availability make them especially attractive for scaling structural energy storage technologies.

Nevertheless, there have been limited studies on how reclaimed CFs perform as battery electrodes, and similarly, the modification of the fiber surface and implications on performance remain largely unknown.<sup>[34,35]</sup> It has been shown that oxidative treatments can lead to an increase in —COOH functional groups, which can store lithium in the form of COO-Li and improve solid electrolyte interphase (SEI) stability and cell capacity.<sup>[36]</sup> In 2017, Zhang and coworkers demonstrated this effect on CF—submerging desized T800 CF in a HNO<sub>3</sub>/H<sub>3</sub>PO<sub>4</sub>/H<sub>2</sub>SO<sub>4</sub> mixture resulted in an increase in specific capacity from around 150 to

200 mAh g<sup>-1</sup>.<sup>[37]</sup> However, these capacities are far from those attained in conventional graphite anodes, which offer excellent high electrochemical performance (350 mAh/g+) at the cost of mechanical strength. Most notably, those treatments tend to etch the fiber surface, and are largely uncontrollable, in that specific functional groups and tailored surface chemistry is not possible. Nevertheless, that work suggested that CF surface chemistry has potential to improve electrochemical performance—and will be further explored in this study.

The fiber surface plays a critical role in both mechanical load transfer and electrochemical stability, presenting an ongoing challenge. In structural batteries, strong interfacial adhesion is essential not only for maintaining mechanical integrity under stress but also for stabilizing the SEI on the CF surface.<sup>[38–40]</sup> This relationship will be further explored in this study. A poorly bonded interface can lead to interfacial debonding, crack propagation, and unstable SEI formation during repeated lithiation/delithiation cycles, ultimately degrading battery performance.

Therefore, in this work, we employed electrochemical surface modification via reduction of aryl diazonium salts,<sup>[41–45]</sup> to functionalize rCF with various functional groups surface (such as NO<sub>2</sub>, NH<sub>2</sub>, SO<sub>3</sub>H, and SH), will be conducted. This work aims to ascertain whether surface chemistry has a measurable impact in LIB anode performance, such as specific capacity (mAh g<sup>-1</sup>) at various C rates and stability of cells after 1000 cycles at 1C rate. This approach supports the development of multifunctional all-fiber structural battery composites, for next generation energy storage systems.

## 2. Experimental Section

### 2.1. Materials

PAN derived T300 Recycled CF fabrics (60 and 200 GSM) were supplied by GEN2Carbon Ltd. (England). Lithium Disks (15.6 mm Diameter × 0.45 mm thickness), polypropylene PP separator (Celgard, 20 µm thickness) 2032 coin cell casings, spring, and spacers were purchased from mKube Enterprise Pty Ltd. Conductive Super P carbon black (CB, ≈40 nm), 4-nitroaniline, 4-aminothiophenol and 4-sulfanilic acid, sodium nitrate, potassium chloride, sulfonic acid, acetonitrile, tetra-*n*-butylammonium hexafluorophosphate, and lithium-hexafluorophosphate solution (LiPF<sub>6</sub> in EC/DEC) were purchased from Sigma Aldrich. Hydrochloric acid (HCl) was attained from Merck (Germany), and ethanol, acetone, and chloroform were acquired from Chem-Supply (Australia).

### 2.2. Electrochemical Grafting

Surface modification of the reclaimed nonwoven fabrics was carried out according to previously reported techniques.<sup>[41–44]</sup> Briefly, the electrolyte solution was prepared as 2 M HCl (225 mL), sodium nitrite (20 mM), and target aniline (15 mM) added and stirred for

15 min. The targeted aniline comprises of 4-aminothiophenol for SH, 4-sulfanilic acid for SO<sub>3</sub>H, and 4-nitroaniline for NO<sub>2</sub>. 60 and 200 GSM nonwoven rCF were used as the working and counter electrode, respectively. The 60 GSM CF is used as the working electrode and thus analyzed in this study, the higher GSM counter electrode ensures that there is enough electroactive area with respect to the working electrode. This higher electroactive surface area ensures that the voltage experienced on the counter is minimal to prevent oxidation side-products.

The carbon fabric was submerged into the prepared solution using a three-electrode cell and a cycling potential (from 0 to  $-1.0$  V vs Ag/AgCl) was applied cyclic voltammetry (CV) conditions (**Figure 1**) with a scan rate of  $10\text{ mV sec}^{-1}$  and ten cycles were used.<sup>[42,43]</sup> After completion, the solution was stirred for 2 min the cycling potential applied again using the same conditions. Finally, the working electrode fabric was extensively washed using three solvents, chloroform, ethanol and acetone, and dried under vacuum overnight at  $70^\circ\text{C}$  to remove all residual solvents. The same procedure was applied without any diazonium salt to attain acid treated CFs as a control. As is often observed, the reduction and subsequent passivation of the electrode surface can be seen at  $\approx -0.5$  V versus reference electrode.<sup>[46,47]</sup>

The amine functionalized CFs were performed according to our previous method.<sup>[48]</sup> For the amine (NH<sub>2</sub>) sample, NO<sub>2</sub>-functionalized CFs were submerged in 225 ml EtOH:H<sub>2</sub>O

(1:9) solution with 0.1 M KCl (1.68 g, 22.5 mmol) added. Using the NO<sub>2</sub>-functionalized CFs as the working electrode, and a 200 GSM CF fabric as the counter, a CV experiment was performed cycling between  $-1.5$  and 0 V versus Ag/AgCl for ten cycles. After completion, the CF was washed extensively with H<sub>2</sub>O, EtOH, and Acetone before drying overnight at  $70^\circ\text{C}$  under vacuum to remove all residual solvents and moisture.

### 2.3. Cell Manufacturing

Surface modified, unmodified, and acid treated 60 GSM CF fabrics were punched into disks and then transferred into an argon glove box with O<sub>2</sub> and H<sub>2</sub>O  $<0.1$  ppm after drying overnight at  $120^\circ\text{C}$ .<sup>[49,50]</sup> A solution of 1 M LiPF<sub>6</sub> (700  $\mu\text{l}$ ) in di-ethylene carbonate (DEC) and ethylene carbonate (EC) (1:1 molar equivalents) was added on top of the CF anode, then a polypropylene separator (M-Kube Enterprise Pty Ltd, 29  $\mu\text{m}$  thickness) was gently placed on top. The assembly of the cell was finalized by sequentially positioning a 15.6 mm diameter Li metal chip (M-Kube Enterprise Pty Ltd, 450  $\mu\text{m}$  thickness), spacer, spring, and the upper casing component. Subsequently, the cell was sealed using a crimping machine to ensure structural integrity. Following an overnight stabilization period, the assembled cell was subjected to performance evaluation using a battery testing system.

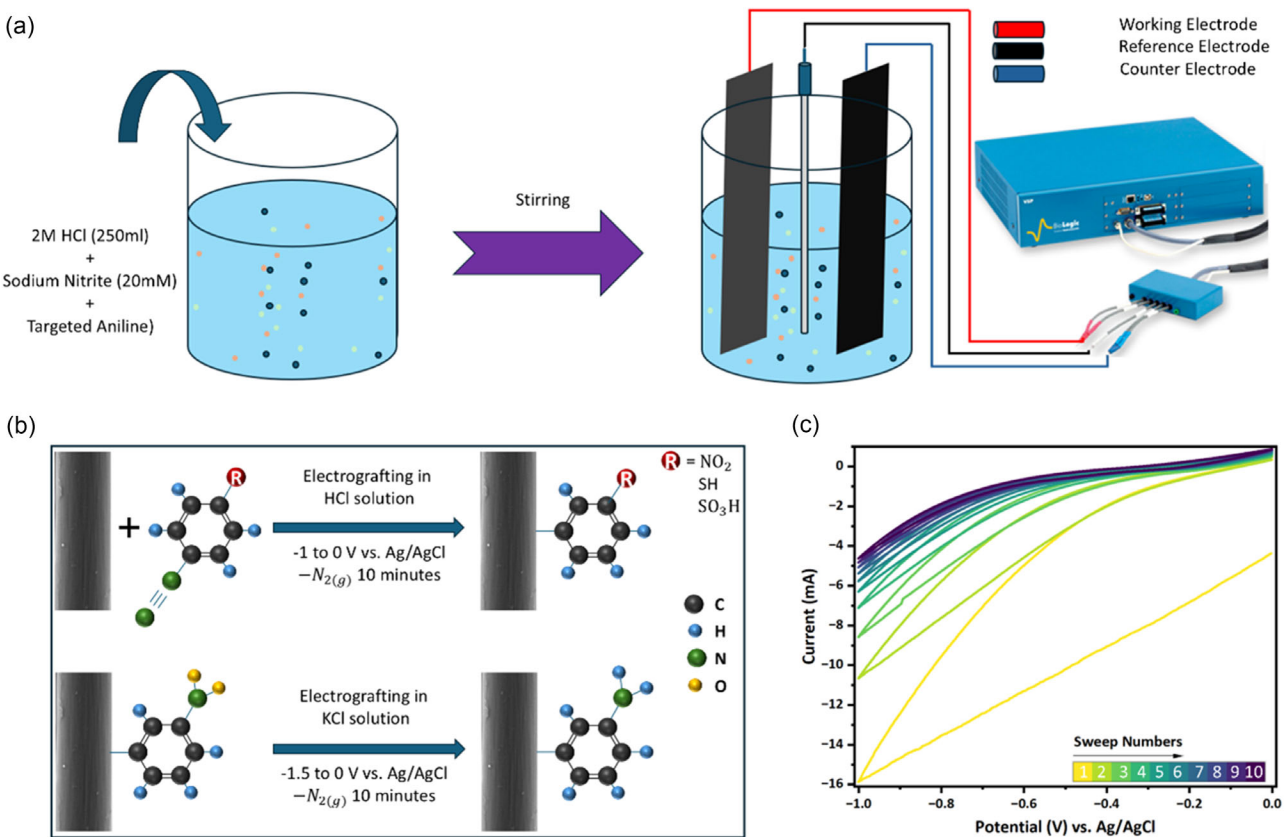


**Figure 1.** a) Experimental setup of electrochemical grafting on 60 GSM rCF fabric by using cycling voltammetry and b) molecular level illustration of electrochemical grafting. c) Cyclic voltammogram of the electrochemical grafting of diazonium salts onto the surface of rCF.

## 2.4. Electrochemical Testing of CF Anodes

Battery tester (Neware A211) and potentiostat (Biologic VMP-300) were used to examine the specific capacity at various C-rates, long term cycling, voltage vs specific capacity, CV curves, and electrochemical impedance spectroscopy (EIS) data.

Galvanostatic charge/discharge (GCD) was conducted using a Neware battery tester (BTS8000), with cycling stability monitored up to 1000 cycles at a 1.0 C. The voltage range was between 0.01 and 1.5 V (vs Li/Li<sup>+</sup>). The selected current for GCD was based on the theoretical capacity of graphite (372 mAh g<sup>-1</sup>) and the mass of the CF anode. Specific capacity of the samples was calculated from the discharge curves as per the formula  $Q = \int Idt/m$ , where  $Q$  is the specific capacity (in mAh g<sup>-1</sup>),  $I$  is the current applied, and  $m$  is the mass of the CF active material.<sup>[51]</sup> Moreover, the Coulombic efficiency (CE) is known as ratio between prepared cell discharge and charge capacity during the same cycle. Hence, CE provides the ratio between total Li-ions insertion into anode material and total Li-ions back to cathode material.<sup>[52]</sup> CV and EIS were conducted on a Bio-Logic SP-300 station. CV of half cells were performed at various scan rates (0.2–409.6 mV s<sup>-1</sup>) with a voltage range of 0–3.0 V (vs Li/Li<sup>+</sup>) for three cycles each. EIS measurements were performed over a frequency region of 100 kHz to 100 mHz using a single sine alternative current.

## 2.5. Scanning Electron Microscopy (SEM)

SEM was employed to investigate the surface morphology of the functionalized CF. Surface characterization was carried out using a field emission scanning electron microscope (JEOL JSM 7800F) operated at an accelerating voltage of 5 kV. The test samples were prepared by mounting single CFs on Al stubs using carbon tape and were imaged without a conductive coating.

## 2.6. Raman Spectroscopy

The Renishaw plc, Gloucestershire (UK) Raman Micro Spectrometer was used to attain spectra of CFs using a 488 nm argon laser. To avoid any structural damage of samples, the laser power was restricted at 10% with 5 accumulations and 10 s exposure time. The Raman spectra were attained from 600 to 2400 cm<sup>-1</sup> using a  $\times 50$  magnification lens and Origin Lab software was used for baseline correction. For each study sample, at least six fibers were used to collect the Raman spectra. The ratio  $I_D/I_G$  was calculated from the D-band peak intensity ( $\approx 1358$  cm<sup>-1</sup>) and G band peak intensity ( $\approx 1573$  cm<sup>-1</sup>).

## 2.7. X-ray Photoelectron Spectroscopy (XPS)

XPS was used to characterize the surface chemical composition of the CF samples using a Thermo Fisher K-Alpha+ XPS/UPS system (Thermo Fisher Scientific, USA). Fiber samples were mounted onto the XPS sample holder by securing both ends with conductive carbon tape. Measurements were performed under ultrahigh vacuum conditions, with a base pressure maintained

at  $\leq 5 \times 10^{-8}$  mbar. The XPS survey spectra were collected from 0 to 1350 eV using a pass energy of 200 eV, a dwell time of 10 ms, and a resolution of 1 eV. High-resolution spectra for C 1s (279–298 eV), O 1s (525–545 eV), and S 2p (157–175 eV) were acquired at a pass energy of 50 eV, a dwell time of 50 ms, and a resolution of 0.1 eV. Each sample was analyzed at three different locations, with ten scans recorded per location to ensure data reproducibility. Spectral analysis and peak fitting of the high-resolution C 1s, O 1s, and S 2p regions, were carried out using CasaXPS (v2.3.22PR1.0) and Avantage (v5.9902) software packages.

## 3. Results and Discussion

The modification of nonwoven reclaimed CF fabrics was undertaken via diazonium-based electrochemical grafting to install nitro, amine, sulfonic acid, and thiol functional groups onto the fiber surface (Figure 1a,b). This method is both facile and rapid, proceeding under mild aqueous conditions and requiring only short electrochemical treatment times, making it highly scalable for industrial application. The nitro, sulfonic acid, and thiol functionalities were introduced using their corresponding aniline precursors, while the amine group was obtained through a post-grafting chemical reduction step using the nitro-functionalized CFs. This was following a protocol form our previous work.<sup>[48]</sup> A sample treated electrochemically in HCl without the aniline precursors was used as a control to ensure that any measurable cell performance deviations were attributable to the surface grafting step. The surface groups were chosen based on their prolific use in the composite space to enhance resin wettability and adhesion in composite systems (NH<sub>2</sub>, NO<sub>2</sub>, and SO<sub>3</sub>H) or to promote some degree of lithiophilic behavior that may assist in SEI formation and stabilization (NH<sub>2</sub>, SH).

After surface modification, analysis by SEM was undertaken to ensure that no surface damage had occurred during the modification process (Figure 2), as this may have major impact on the physical and electrochemical properties of these materials and their subsequent ability to act as structural reinforcements.

SEM micrographs of the unmodified and modified CFs show little discernible differences in surface morphology with the diameter of all fibers being  $\approx 6$ –7  $\mu$ m. No obvious defects on any treated samples were observed, reinforcing the gentle nature of this modification and is consistent with earlier reports.<sup>[41–44]</sup> In our previous work, we have shown that no differences in microstructure is measured through atomic force microscopy roughness mapping.<sup>[45]</sup> Similarly, the surface characterization of the modified fibers was carried out using Raman and XPS.

The Raman spectra (Figure 3) of unmodified and surface modified CFs, with each CF spectrum present two characteristics bands, D-band ( $\approx 1358$  cm<sup>-1</sup>) and G-band ( $\approx 1573$  cm<sup>-1</sup>), which are associated with disordered carbon structure (D-band) and graphitic structure (G-band) of carbon, respectively.<sup>[47,53]</sup> Although the unmodified CF reveals a strong D-band attributed to defects in the structure of rCF, intensity ratios of  $I_D/I_G$  for unmodified CF (0.91) are lowest among other surface treated samples. The SH-grafted CF has highest  $I_D/I_G$  ratio (0.95) and is attributed to

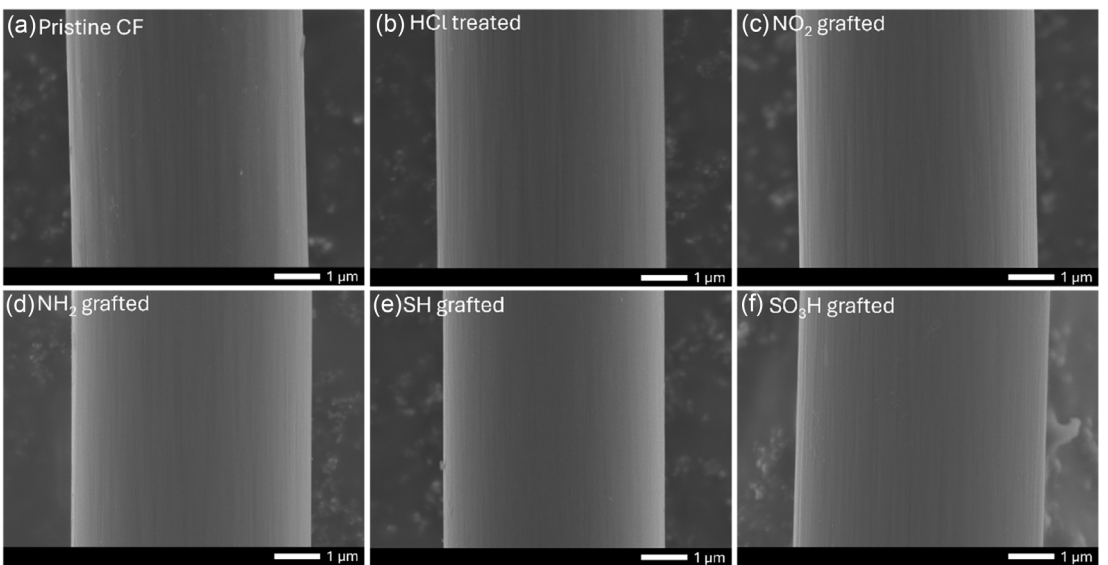


**Figure 2.** a-f) SEM images of unmodified CF, HCl treated,  $\text{NO}_2$  grafted, and  $\text{NH}_2$ , SH, and  $\text{SO}_3\text{H}$  modified, respectively.

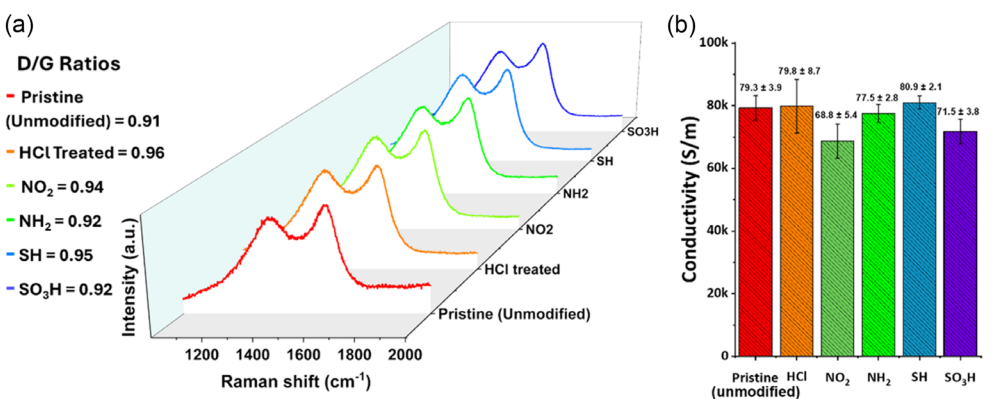


**Figure 3.** a) First order Raman spectra of unmodified and surface treated CFs and spectral region  $I_D/I_G$  ratios. b) 4-point probe conductivity measurements of modified and unmodified CFs.

more disruption in the  $\text{sp}^2$  bonds of the CF, suggesting greater grafting density for this sample.<sup>[53,54]</sup> Chaudhuri et al.<sup>[55]</sup> has reported the interfacial debonds between CFs and polymer resin matrix and mentioned that higher value of  $I_D/I_G$  ratio provided higher degree of functionalization. Therefore, compared to pure CF  $I_D/I_G$  ratio, the surface modified CFs have 0.92–0.95  $I_D/I_G$  ratio which is good evidence of grafting success of desired functional groups.

As poor electrical conductivity of the anode can greatly influence charge transfer resistance ( $R_{\text{ct}}$ ), electrical conductivity measurements were performed on the modified and unmodified CF substrates (Figure 3b). Since diazonium grafting reactions interrupt aromaticity and generate  $\text{sp}^3$ -hybridized carbon at the surface, some degree of resistance buildup might be expected during electrochemical modification. The electrical conductivity was measured along the fiber length using the four-point probe method, whereby pristine CFs exhibited a conductivity of  $79.3 \pm 3.9 \text{ S m}^{-1}$ , while the HCl-treated fibers showed

a similar value of  $79.8 \pm 8.7 \text{ S m}^{-1}$ . Among the modified samples, SH-functionalized CFs achieved the highest conductivity ( $80.9 \pm 2.1 \text{ S m}^{-1}$ ), closely matching pristine fibers. The  $\text{NO}_2$ - and  $\text{SO}_3\text{H}$ -modified CFs displayed slightly lower conductivities of  $68.8 \pm 5.4$  and  $71.5 \pm 3.8 \text{ S m}^{-1}$ , respectively, while  $\text{NH}_2$ -modified CFs measured  $77.5 \pm 2.8 \text{ S m}^{-1}$ . These modest differences are more likely due to microstructural heterogeneity among filaments rather than the grafting process itself. Overall, the results confirm that surface modification did not significantly alter the electrical conductivity of CFs, indicating that the bulk fiber intrinsic electrical behavior was preserved after treatment.

Following this, confirmation of chemical grafting was established through XPS analysis, as evidenced by changes in bonding states observed in the high-resolution C 1s spectra (Figure 4) and the elemental compositions derived from the XPS survey spectra (Table 1). Deconvolution of the C 1s spectra revealed an asymmetric C—C/C—CH peak at 284.8 eV, corresponding to  $\text{sp}^2$ - and  $\text{sp}^3$ - hybridized carbon species characteristic of the

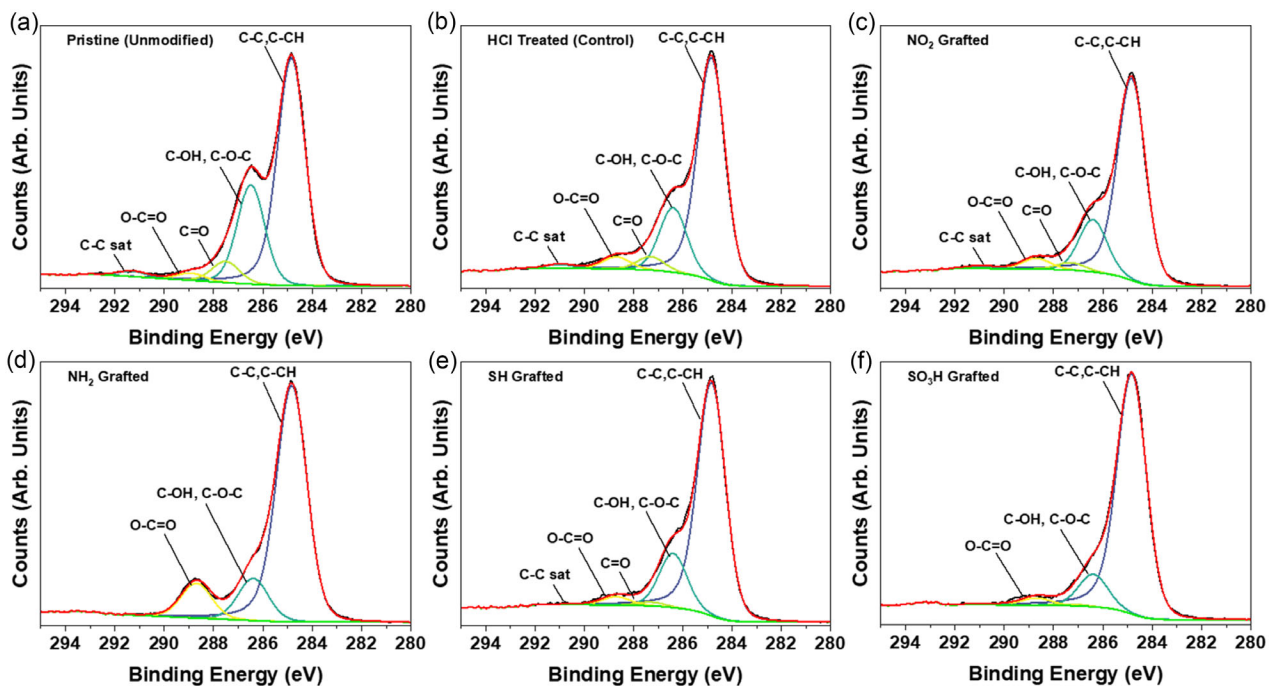


**Figure 4.** Peak-fitted high-resolution C 1s spectra of a) unmodified rCF, b) HCl-treated CF, and electrochemically modified rCF samples grafted with c)  $\text{NO}_2$ , d)  $\text{NH}_2$ , e) SH, and f)  $\text{SO}_3\text{H}$  functional groups.

**Table 1.** Relative abundances of carbon bonding species derived from high-resolution C 1s XPS spectra. Note: atomic percentages are rounded to one decimal place; total may not equal exactly 100% due to rounding.

Sample ID	Peak area percentage [%]				
	C-C/ C-CH	C-OH/ C-O-C	C=O	O-C=O	C-C Satellite
Pristine (Unmodified)	64.3%	26.6%	5.7%	2.0%	1.5%
HCl treated (Control)	71.4%	19.7%	4.1%	3.7%	1.2%
$\text{NO}_2$ grafted	74.5%	18.3%	2.6%	3.7%	0.9%
$\text{NH}_2$ grafted	76.2%	13.1%	0.0%	10.7%	0.0%
SH grafted	78.6%	17.4%	1.2%	2.7%	0.1%
$\text{SO}_3\text{H}$ grafted	85.8%	11.0%	0.6%	2.4%	0.2%

graphitic structures of CFs.<sup>[56–59]</sup> Additionally, a peak at 286.5 eV was attributed to C=O bonds, likely originating from oxygenated alcohol (C-OH) and ester (C-O-C) groups, which are typically generated via electrochemical oxidation during the CF manufacturing process.<sup>[59–61]</sup> Peaks assigned to other oxygen-containing functional groups, such as C=O and O-C=O, were observed at 287.5 and 288.9 eV, respectively.<sup>[59–62]</sup>

Notably, the diazonium grafting reaction typically occurs via the formation of a  $\text{sp}^3$ -hybridized carbon bond by reacting with  $\text{sp}^2$ -hybridized carbon sites that may rearomatize.<sup>[63]</sup> In our previous work, we have typically performed the diazonium grafting step using CFs that have not undergone any electrochemical oxidation treatment. Thus, we were interested in assessing whether oxygenated rCFs were amenable to the *in situ* diazonium grafting despite possessing reduced  $\text{sp}^2$  carbon content.<sup>[54]</sup>

Analysis of the peak-fitted C 1s spectrum of the pristine CF (Figure 4a) shows higher oxygen content compared to the other samples, as indicated by a notably higher C-OH/C-O-C peak percentage of 26.58%, compared to 19.66% in the HCl-treated control (Table 1). As reclaimed CFs undergo a secondary pyrolysis step in air to remove surface adhered char, it is likely that a small amount of residual oxidized amorphous carbon remained embedded in the graphitic planes of the CF and was detectable through XPS (surface penetration of  $\approx 10$  nm), but not by Raman or SEM. Minimizing this char layer during CF composite recycling is well reported in the literature, however not to the extent of complete elimination.<sup>[64–66]</sup>

The presence of this additional surface layer is further supported by the counterintuitive decrease in elemental O% (4.05%) (Table 2) and the reduced relative abundance of C-OH/C-O-C species (6.92%) in the HCl treated control sample relative to the unmodified CF. This suggests that electrochemical treatment of

**Table 2.** Surface elemental composition of samples determined from the XPS survey spectra. Note: atomic percentages are rounded to one decimal place; total may not equal exactly 100% due to rounding.

Sample ID	Atomic elemental surface composition [at.%]				
	C	O	N	F	S
Pristine (unmodified)	81.5%	16.7%	1.0%	0.8%	0.0%
HCl treated (control)	82.8%	13.7%	2.6%	0.9%	0.0%
$\text{NO}_2$ grafted	82.0%	13.3%	3.2%	1.5%	0.0%
$\text{NH}_2$ grafted	79.1%	16.6%	4.3%	0.00%	0.00%
SH grafted	81.3%	13.7%	3.1%	0.00%	1.9%
$\text{SO}_3\text{H}$ grafted	69.0%	23.4%	2.4%	0.4%	4.9%

the fibers in 2 M HCl and 5 mM NaNO<sub>2</sub> assists in removing adsorbed char debris. Despite this, all samples show an increase in C—C/C—CH content after exposure to the targeted aniline relative to the HCl-treated control sample. Moreover, this increase in C—C/C—H bonding abundance meant that the formation of additional C—C bonds has occurred and is a supportive indicator of grafting success.

Evidence for grafting success of the sulfur-containing moieties is highlighted in the increase in S% (Table 1), along with the evolution of S-based peaks from the high-resolution S 2p spectra (**Figure 5**) in the thiol (SH) and sulfonic acid (SO<sub>3</sub>H) modified samples. Specifically, sulfur was identified in both SH (1.93%) and SO<sub>3</sub>H (4.81%) grafted samples, whereas no sulfur content was measured in the survey scan of any of the other tested samples.

The peak-fitted high-resolution S 2p spectra of the thiol-grafted CF (Figure 5a) shows two distinct regions of interest. The first region, spanning 163–165 eV, comprises a prominent doublet that can be deconvoluted into S 2p<sub>3/2</sub> and S 2p<sub>1/2</sub> components, corresponding to sulfur-containing groups in neutral environments such as S—H, S—C, and S—S.<sup>[67,68]</sup> The S 2p<sub>3/2</sub> peak has double peak area percentage as the S 2p<sub>1/2</sub> due to spin-orbit coupling, which splits the sulfur 2p level into two states with a 2:1 degeneracy ratio. The second region features a smaller peak at ≈168 eV, indicative of oxidized sulfur moieties in higher oxidation states, including SO<sub>3</sub>H, SO<sub>3</sub><sup>−</sup>, and SO<sub>4</sub><sup>2−</sup>. The predominance of the sulfur species at lower binding energies supports the successful grafting of thiol groups onto the CF surface.

In contrast, the high-resolution S 2p spectrum of the sulfonic acid-grafted sample (Figure 5b) exhibits only the second region, with peaks in the 168–169 eV range, characteristic of oxidized sulfur species such as SO<sub>3</sub>H, SO<sub>3</sub><sup>−</sup>, and SO<sub>4</sub><sup>2−</sup> species. However, due

to the minimal differences in binding energies among these S—O species, individual peak resolution through deconvolution is not feasible.<sup>[67,68]</sup> Nevertheless, the exclusive presence of this higher binding energy region strongly suggests that the grafted sulfur exists primarily as sulfonic acid rather than thiol. These spectral features provide additional confirmation of successful surface functionalization. Collectively, these findings affirm the effectiveness of the grafting process and lay the groundwork for evaluating the electrochemical performance of the modified CF samples.

### 3.1. Electrochemical Evaluation of Modified CFs

To fully observe the ability of the anode material to store lithium ions, half cells were fabricated using the free-standing CF fabric as the working electrode and lithium metal chips as the counter electrode. It is worth noting that no copper foil was used in the manufacturing process, as the free-standing nature of the nonwoven rCFs ensured good contact to the steel casing throughout the electrochemical evaluation.

Long-term cycling at 1C shows stable capacity retention with initial capacities ranging from ≈30 to 140 mAh g<sup>−1</sup> (**Figure 6**), with Columbic efficiencies averaging ≈100% for all samples. Interestingly, the unmodified fibers showed the lowest initial specific capacity, however rose over the course of 300 cycles, before gradually decreasing. Our initial hypothesis was that the removal of residual, electrochemically inactive amorphous carbon—likely remaining from the pyrolysis reclamation process—may enhance lithium intercalation, which is otherwise hindered in early cycles. During cycling, fiber expansion may dislodge this residual carbon, thereby exposing new intercalation sites. A similar phenomenon was reported by Zhang et al. who observed improved performance in pristine CFs cycled in a comparable electrolyte (LiPF<sub>6</sub> in EC:DMC:EMC, 1:1:1 vol).<sup>[69]</sup> They attributed the effect to electrochemical activation and/or increased ionic accessibility. We support this interpretation. Notably, this behavior was not observed in the HCl-treated control fibers, suggesting that electrochemical surface treatment facilitates the removal of residual carbon prior to cycling. Ultimately, the mild electrochemical grafting in HCl/NaNO<sub>2</sub> contributes to improved initial cycling stability. Furthermore, SH modified CFs showed the highest specific capacity (≈80 mAh g<sup>−1</sup>), while the NH<sub>2</sub> and NO<sub>2</sub> fibers displayed the lowest (≈20 mAh g<sup>−1</sup>) after 1000 cycles. The high performance of the thiol modified fiber may be due to SH functional groups which have been shown to facilitate a more stable SEI with a decreased Li-ion transfer barrier.<sup>[56]</sup> The lower performance of the aminated surface may be attributed to surface reactions involved with the electrolyte, leading to excessive breakdown and is discussed further on.

For high-rate applications, considering the turbostratic structure is required in structural batteries (lithium-based cells),<sup>[70]</sup> the rate capability was analyzed to calculate the specific capacity of unmodified and modified CF electrodes at various C-rates. The unmodified CF anode (**Figure 6a**) has a reversible and irreversible specific capacity of almost 140 and 35 mAh g<sup>−1</sup>, respectively. Kjell et al.<sup>[71]</sup> investigated the electrochemical performance of

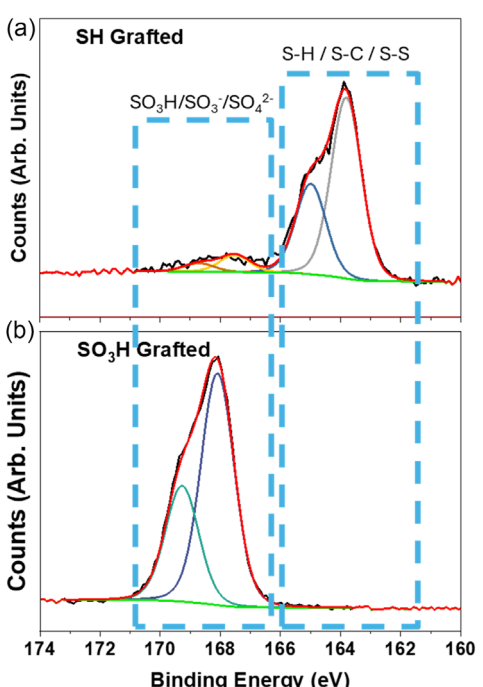


**Figure 5.** Peak-fitted high-resolution XPS spectra of a) functionalized SH and b) SO<sub>3</sub>H-modified CF samples.

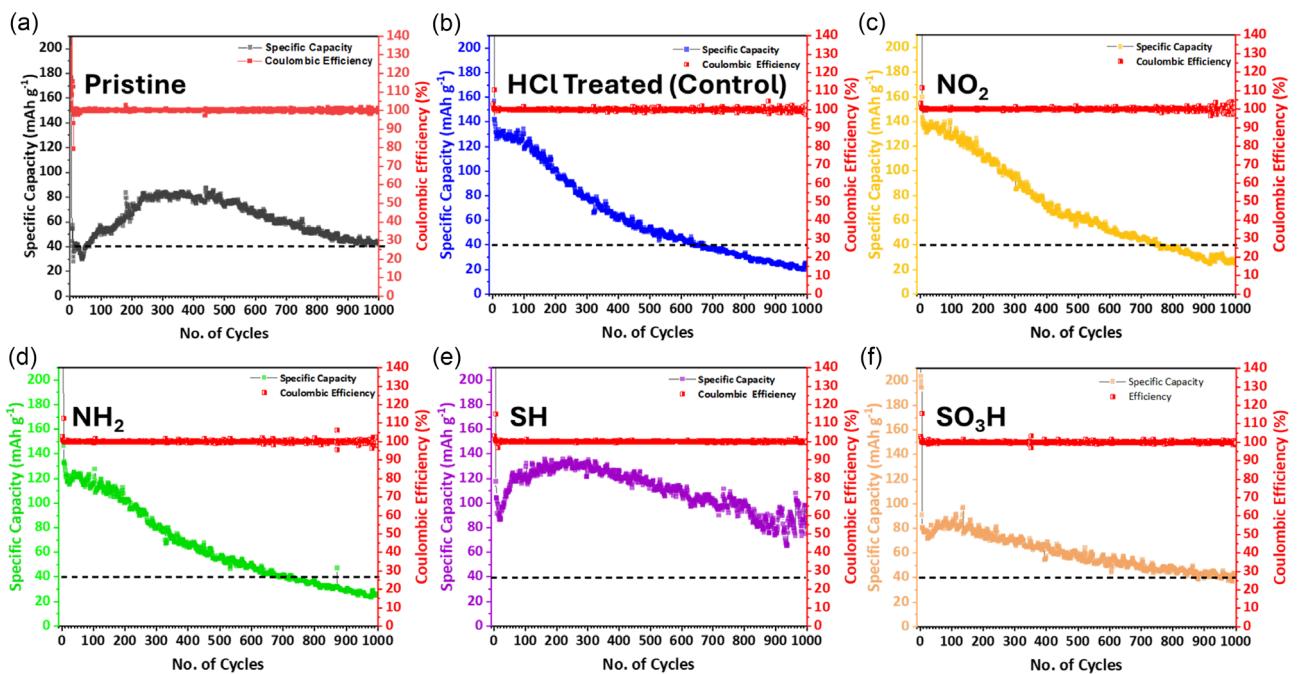


**Figure 6.** Specific capacity and efficiency versus 1000 cycles at 1C-rate of prepared CF anodes a) Pristine (unmodified), b) HCl treated (Control), c)  $\text{NO}_2$  treated, d)  $\text{NH}_2$  treated, e) SH treated and f)  $\text{SO}_3\text{H}$  treated. The dotted line is at  $40 \text{ mAh g}^{-1}$  to give context for pristine (unmodified) fibers.

carbon fiber anodes with and without surface sizing (referred to as sized and desized fibers, respectively). They reported that, at a C/10 charge rate, most of these fiber-based electrodes exhibited reversible capacities of  $\approx 100 \text{ mAh g}^{-1}$ . This is in good agreement with the capacities observed in our study. The irreversible capacity is manifested during first few cycles and is attributed to SEI layer formation and side reactions with electrolyte components.<sup>[72–74]</sup> The irreversible specific capacity values at C/10 for all samples lie between 10 and  $45 \text{ mAh g}^{-1}$ , with the exception of  $\text{NO}_2$  and  $\text{NH}_2$  samples which displayed an irreversible capacity of  $94.2\text{--}88.6 \text{ mAh g}^{-1}$ , respectively, after the first charge, suggesting more electrolyte consumption occurring during SEI formation.<sup>[56]</sup> This higher irreversible capacity after the first charge may have negative implications in solid polymer electrolyte systems, as more electrolyte is needed in order to stabilize the anode. This will then reduce the available lithium inventory within the cell and have direct consequences in the cycle life and battery efficiency of the final cell. Implications of excessive electrolyte consumption can be observed in Figure 6, where the final capacity of the  $\text{NH}_2$  and  $\text{NO}_2$  surfaces were the lowest amongst the other samples.

Similar to the long-term cycling measurements rate capability performance of the modified CFs show significant capacity improvements relative to the unmodified samples (Figure 7), a decreasing specific capacitance along an increasing C-rate is generally manifested due to Li-ions diffusion and electrons transport limitations via electrode material.<sup>[69]</sup> Initial charge capacity for the unmodified CF was measured at  $189.1 \pm 42.6 \text{ mAh g}^{-1}$ , with the SH and  $\text{NO}_2$  modified fibers showing the highest initial specific capacity of  $244.0 \pm 12.1$  and  $243.8 \pm 64.1 \text{ mAh g}^{-1}$ . Interestingly, the thiol modified CFs displayed the highest

capacity at C/10 after 50 cycles with a recorded specific capacitance of  $263.4 \pm 46.4 \text{ mAh g}^{-1}$ , suggesting that during the cycling process stabilization additional capacity was attained. The climb in capacity can also be observed in the long-term cycling data (Figure 6e). Another interesting observation was the low performance of the  $\text{SO}_3\text{H}$  samples, which performed at around the same specific capacity as the unmodified samples, suggesting that the sulfonic acid does not contribute in any meaningful manner to the electrochemical performance. Voltage profiles of the surface modified electrodes looked largely the same in comparison to the unmodified, however the SH and the sulfonic acid modified electrodes all showed an increase in the charge and discharge capacities for the 10th cycle in respect to the second cycle.

In general, a  $\approx 15\%$  improvement in the specific charge capacity at C/10 after the rCFs underwent electrochemical surface modification (Figure 7b). These improvements became more pronounced at higher 1 and 2C charge rates, where an  $\approx 44\%$  and  $63\%$  improvement were observed, respectively. It is evident that a major source of capacity improvements was attained through beneficial interactions of the HCl and  $\text{NaNO}_2$  to the CF surface, however, further increases and retention of capacity in electrochemical performance were realized through the grafting of the diazonium species, specifically the thiol. An exception is presented in the  $\text{SO}_3\text{H}$  grafted sample, which appears to have negated the performance improvements offered by the HCl/ $\text{NaNO}_2$ . Another interesting feature that was observed in all samples was the increase in voltage during the initial first discharge cycle (Figure 7c-h). One possible explanation is that surface activation occurs during this stage, enhancing SEI formation and increasing ionic accessibility, which results in a slight voltage

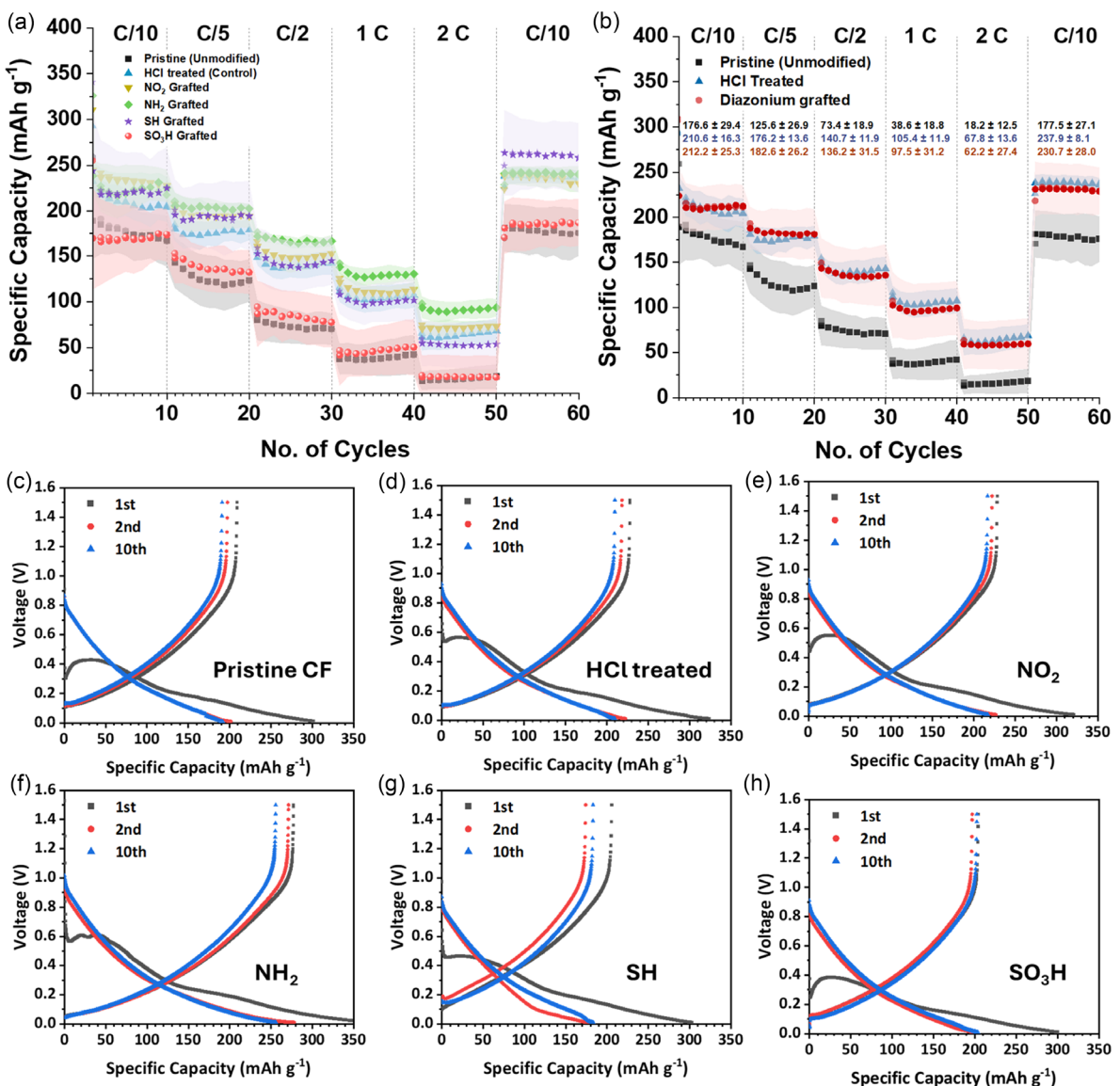


**Figure 7.** a) Specific capacities at various C-rates, and b) distribution of specific capacities versus number of cycles. c–h) Potential versus capacity graphs of first, second and 10th cycle at ambient temperature of unmodified and surface modified CF anodes at 0.1 C-rate.

rise before stabilization. As this effect occurs independently of the grafted functional groups, it is likely related to electrolyte interactions that are intrinsic to carbon, such as surface morphology or electrochemical activation, rather than the specific chemical functionalities.

CV experiments were performed at various scan rates to ensure that no unexpected redox activity was taking place and to better understand lithiation kinetics (**Figure 8a**). Analysis of the peak intensities against the scan rate displayed 2 distinct slopes for all samples (**Figure 8b–d**), corresponding to a shift in lithiation rate occurring at  $0.1\text{--}2.0\text{ (mV s}^{-1}\text{)}^{1/2}$ , after which a shallower slope is observed. At these slow rates, lithium-ion diffusion is sufficiently fast to allow effective intercalation into the carbon fibers without being rate-limiting. However, at higher rates, transport limitations and bottlenecks at the surface or within the fiber structure may hinder lithiation.

The rate at which this shift in slope occurs is at  $\approx 2.5\text{ (mV s}^{-1}\text{)}^{1/2}$  (**Figure 8b**), where Li<sup>+</sup> ions require time to intercalate further before surface sites are regenerated allowing for more intercalation. The SH modified fibers displayed the steepest slope ( $K_a = 0.102$ ) at low scan rates, indicating enhanced lithium accessibility or improved surface kinetics. As was consistent with the rate cycling and long-term experiments, the SO<sub>3</sub>H modified CFs showed the lowest slope ( $K_a = 0.077$ ), suggesting transport limitations into the CFs, and the unmodified CFs showed a marginally steeper slope ( $K_a = 0.088$ ).

To better understand the influence of surface chemistry after cycling, XPS analysis was performed on SH-modified fibers after 1000 cycles (**Figure 9**). As expected, an SEI film formed on the CF throughout cycling, dominated by carbonate and alkyl carbonate species. However, a faint S 2p doublet was also still visible at  $\approx 163\text{--}164\text{ eV}$ , suggesting a fraction of the thiol-derived

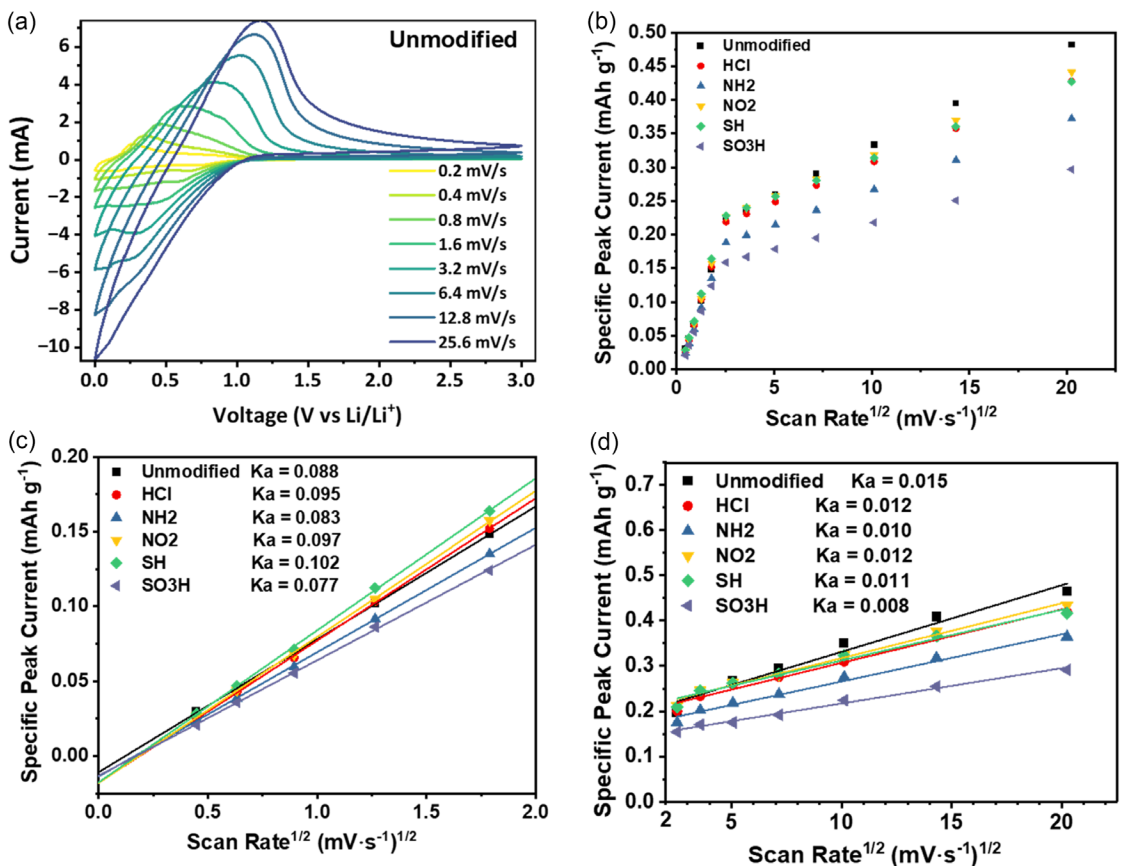


**Figure 8.** a) CV curves of prepared half-coin cells (V vs Li/Li<sup>+</sup>) at various scan rates (0.2–25.6 mV s<sup>-1</sup>). b-d) Randles-Ševčík plots of modified samples at various scan rates.

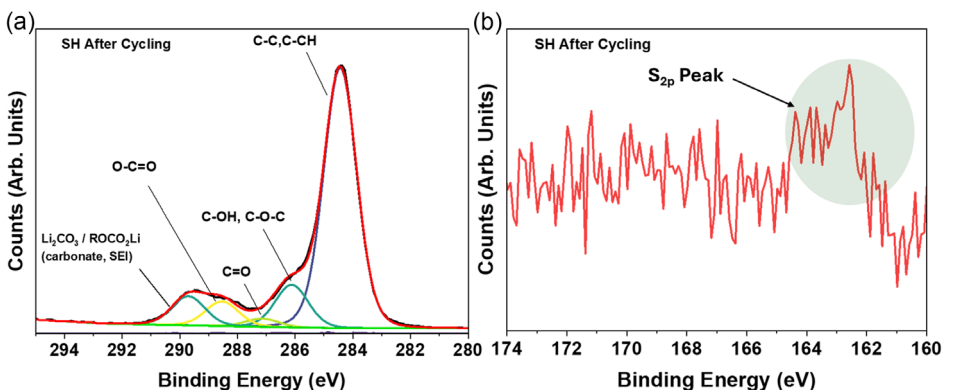


**Figure 9.** a) High-resolution C 1s spectrum of SH-modified CF after cycling, showing dominant SEI components including C—C/C—H, C—O, O—C=O, and carbonate species ( $\text{Li}_2\text{CO}_3/\text{ROCO}_2\text{Li}$  (carbonate, SEI)). b) High-resolution S 2p spectrum of the same sample after 1000 cycles, where a faint S 2p doublet remains ( $\approx 163$ –164 eV) despite being largely masked by SEI contributions, suggesting partial retention of thiol-derived sulfur beneath a relatively thin SEI.

surface chemistry remains detectable despite extensive SEI coverage. While in this case full deconvolution of thiol versus oxidized sulfur species is challenging due to overlap with SEI components, these results indicate that the SEI film on SH modified fibers is relatively thin (<10 nm). More advanced techniques such as depth-profiling XPS or transmission electron microscopy could provide greater insight into thiol stability under cycling, which we highlight as an avenue for future work.

Internal resistances of the half cells was characterized through EIS (10 mHz to 100 kHz) (Figure 10). In the resulting Nyquist plots, the electrolyte resistance ( $R_s$ ) is represented by the intercept at high frequency on the real axis, while the charge transfer resistance ( $R_{ct}$ ) corresponds to the diameter of the semicircle in the high-to-mid frequency region.<sup>[75,76]</sup> The EIS impedance values before SEI formation shows a very steep inductive rise in the mid-low frequency regions for all samples, this rise is attributed

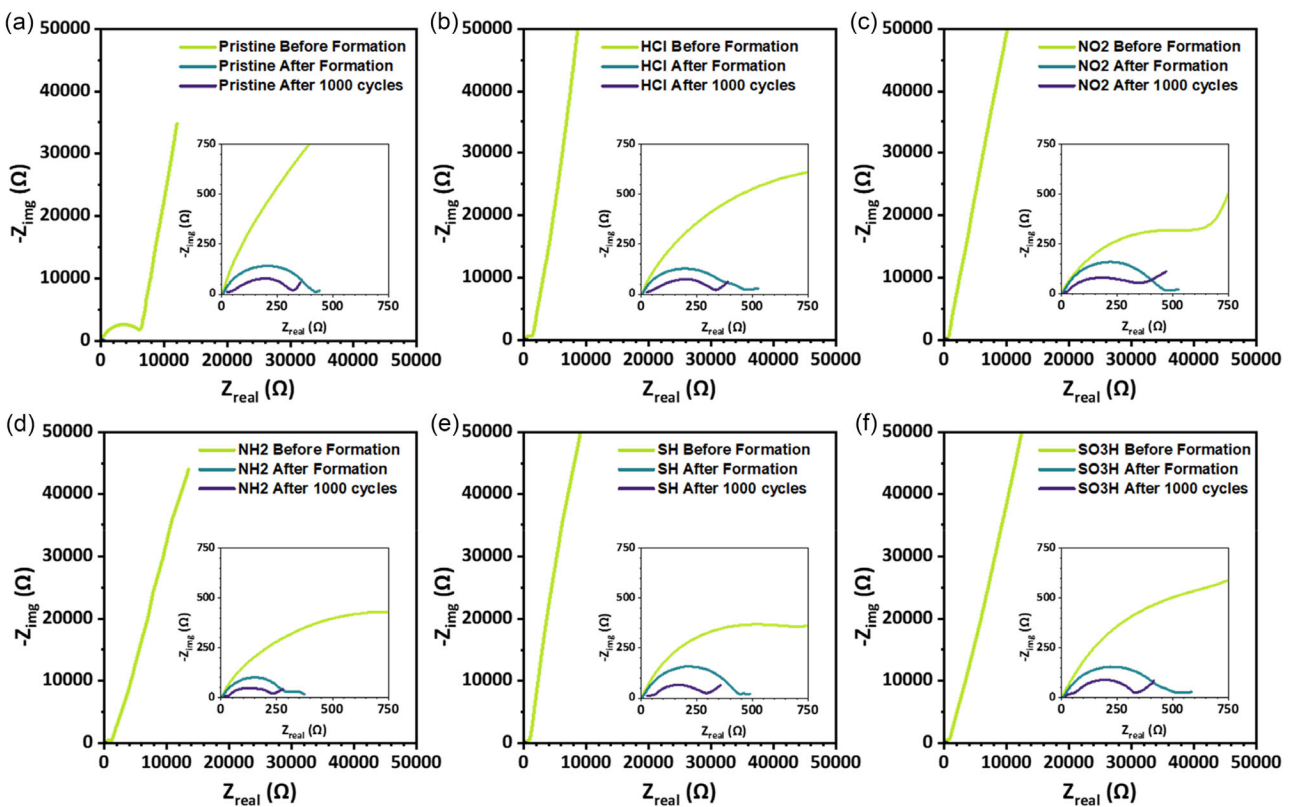


**Figure 10.** EIS impedance spectra of studies samples at various stages of cycling. a) pristine (unmodified), b) HCl treated (control), c)  $\text{NO}_2$  treated, d)  $\text{NH}_2$  treated, e) SH treated and f)  $\text{SO}_3\text{H}$  treated. Green line occurring before formation (24 h after cell assembly), blue line occurring after 5 formation cycles at C/10, and purple after 1000 cycles.

to the absence of a stable SEI layer. As the SEI forms during initial cycling, passivation of the CF surface occurs with an ionically conductive SEI film that leads to a substantial decrease in interfacial resistance and more stable impedance characteristics.<sup>[76–79]</sup> Interestingly, the pristine fiber shows a very large arc in the high-frequency region which is suggestive of additional interfacial resistances attributable to the formation of an additional interface layer (Figure 10a). However, this may also be due to reduction of electrolyte components.<sup>[77]</sup> After formation, resistances are highest for the HCl treated and  $\text{SO}_3\text{H}$  samples which are about 475–500  $\Omega$  (Figure 10b,f ). This agrees well with the data where HCl treated and  $\text{SO}_3\text{H}$  half cells provide lower capacity at 1C rate (Figure 6). The Impedance values for other samples vary between 290 and 450  $\Omega$ .

After 1000 cycles, it can be observed that the impedance decreases for all half-cells (Figure 10) suggesting stabilization of the SEI layer over cycling. The decrease in specific capacity must therefore come from factors such as electrode fracture that leads to a reduction in active sites. The impedance values for  $\text{NO}_2$ ,  $\text{SO}_3\text{H}$ , and HCl treated samples are larger than other half cells in the higher frequency regions. Usually, the high frequency region semi-circle presents the transfer resistance of  $\text{Li}^+$  in electrolyte as well as the interface resistance due to SEI layer. Therefore, the interfacial impedance of  $\text{NO}_2$  and  $\text{SO}_3\text{H}$  anodes produced by SEI layer is higher than other samples after 1000 cycles attributed to a thick layer of SEI on these electrodes'

surface<sup>[80]</sup> and again is consistent with the rate cycling data presented above (Figure 7).

#### 4. Conclusion

This study on modified CFs shows valuable insights on the impact of fiber surface chemistry on electrochemical battery performance. Most importantly, variances in electrochemical performance through the grafting various functional groups onto the surface of CFs was observed relative to the specific functional group chemistry. Functional groups that have been reported to improve mechanical performance and resin wettability in conventional composite systems (such as,  $\text{NH}_2$  and SH) offer no negative impact on battery performance, and in the case of SH, improved the capacity and rate cycling behavior of these electrodes. Long term cycling at 1C showed that the unmodified CFs exhibiting an increase in capacity up to around 200 cycles followed by a reduction. This is contrasted with all other surface treated fibers exhibiting mostly linear capacity fade. The lithophilic thiol modified CFs exhibited the highest long-term cycling performance with a final specific capacity of 82  $\text{mAh g}^{-1}$  after 1000 cycles and was attributed to an improved solid–electrolyte interface. In contrast, the sulfonic acid functionalized CFs showed the lowest capacity at around 20  $\text{mAh g}^{-1}$ . Rate capability measurements also positioned the thiol modified CFs as the highest

performance surface chemistry, which was supported by EIS and CV rate analysis.

## Acknowledgements

The authors gratefully acknowledge Deakin University, this research was conducted with support from the Australian Research Council Industry Transformation Research Hub (IH210100023), Discovery Projects (DP180100094, DP200100090, and DP230100587), and an IM Fellowship (IM230100048) for LH. This work was also partially supported by the Office of Naval Research (N62909-22-1-2052). The authors also acknowledge the facilities, and the scientific and technical assistance, of Microscopy Australia (formerly known as AMMRF) and the Australian National Fabrication Facility (ANFF). Gen2Carbon is thanked for providing reclaimed fiber fabrics. Leif Asp and Ruben Tavano acknowledge funding from the Office of Naval Research, ONR, Contract No. N62909-22-1-2035.

## Conflict of Interest

The authors declare no conflict of interest.

## Author Contributions

**Muhammad Aqeel:** data curation (lead); formal analysis (lead); writing—original draft (equal); writing—review and editing (equal). **Bhagya Dharmasiri:** formal analysis (supporting); supervision (supporting); writing—original draft (equal); writing—review and editing (equal). **Ruben Tavano:** formal analysis (supporting); visualization (supporting); writing—review and editing (supporting). **Elmer Austria:** data curation (lead); formal analysis (lead); writing—original draft (lead); writing—review and editing (lead). **Behnam Akhavan:** formal analysis (equal); supervision (supporting); writing—review and editing (equal). **Leif E. Asp:** conceptualization (supporting); writing—review and editing (supporting). **Luke C. Henderson:** conceptualization (lead); funding acquisition (lead); project administration (lead); supervision (equal); writing—original draft (supporting); writing—review and editing (supporting). **James D. Randall:** data curation (supporting); formal analysis (supporting); investigation (equal); supervision (lead); visualization (supporting); writing—original draft (equal); writing—review and editing (equal).

## Data Availability Statement

The data that support the findings of this study are available in the supplementary material of this article.

**Keywords:** battery · interface · reclaimed carbon fiber · surface chemistry

- [1] X. Wang, X. Dong, Z. Zhang, Y. Wang, *J. Traffic Transp. Eng., Engl. Ed.* **2024**, *11*, 1340.
- [2] J. Wang, W. Azam, *Geosci. Front.* **2024**, *15*, 101757.
- [3] N. An-Giang, V. Rakesh, N. D. Pravin, P. Chan-Jin, *Energy Mater.* **2023**, *3*, 300030.
- [4] W. Ruo, W. Haonan, Z. Huajun, Y. Mingman, L. Zhongbo, Z. Guangzhao, Z. Tong, Q. Yunxian, W. Jun, L. Iseult, D. Yonghong, *Energy Mater.* **2023**, *3*, 300040.
- [5] J. M. Luk, H. C. Kim, R. De Kleine, T. J. Wallington, H. L. MacLean, *Environ. Sci. Technol.* **2017**, *51*, 8215.
- [6] G. Refiadi, I. S. Aisyah, J. P. Siregar, *Automot. Exp.* **2019**, *2*, 78.
- [7] F. Czerwinski, *Materials* **2021**, *14*, 6631.
- [8] J. T. J. Burd, E. A. Moore, H. Ezzat, R. Kirchain, R. Roth, *Appl. Energy.* **2021**, *283*, 116269.
- [9] N. Akhil, M. Srikanth, C. Ying, S. Neeraj, H. Qi, R. M. Mokhlesur, *Energy Mater.* **2024**, *4*, 400064.
- [10] H. Zhou, H. Li, L. Li, T. Liu, G. Chen, Y. Zhu, L. Zhou, H. Huang, *Mater. Today Energy* **2022**, *24*, 100924.
- [11] B. J. Hopkins, J. W. Long, D. R. Rolison, J. F. Parker, *Joule.* **2020**, *4*, 2240.
- [12] P. U. Nzereogu, A. D. Omah, F. I. Ezema, E. I. Iwuoha, A. C. Nwanya, *Appl. Surf. Sci. Adv.* **2022**, *9*, 100233.
- [13] R. Chaudhary, J. Xu, Z. Xia, L. E. Asp, *Adv. Mater.* **2024**, *36*, 2409725.
- [14] W. Johannisson, D. Zenkert, G. Lindbergh, *Multifunct. Mater.* **2019**, *2*, 035002.
- [15] J. F. Snyder, E. L. Wong, C. W. Hubbard, *J. Electrochem. Soc.* **2009**, *156*, A215.
- [16] Y. Fu, Q. Gan, *J. Solid State Electrochem.* **2023**, *27*, 345.
- [17] B. Nie, J. Lim, T. Liu, I. Kovalenko, K. Guo, J. Liang, J. Zhu, H. Sun, *Battery Energy.* **2023**, *2*, 20230023.
- [18] G. J. H. Lim, K. K. Chan, N. A. A. Sutrisnoh, M. Srinivasan, *Mater. Today Sustain.* **2022**, *20*, 100252.
- [19] S. Chen, L. Qiu, H.-M. Cheng, *Chem. Rev.* **2020**, *120*, 2811.
- [20] L. E. Asp, M. Johansson, G. Lindbergh, J. Xu, D. Zenkert, *Funct. Compos. Struct.* **2019**, *1*, 042001.
- [21] R. Gray, T. Bartheley, C. R. Bowen, F. Marken, A. J. G. Lunt, L. E. Asp, D. Zenkert, P. S. Rodriguez, J. Xu, K. Bouton, A. T. Rhead, *J. Mater. Chem. A* **2024**, *12*, 25580.
- [22] B. Liu, Q. Gan, Y. Fu, *RSC Adv.* **2024**, *14*, 6462.
- [23] J. Liu, X. Chen, D. Liang, Q. Xie, *Energy Sources, Part A.* **2024**, *46*, 14492.
- [24] D. Zhao, L. Wang, P. Yu, L. Zhao, C. Tian, W. Zhou, L. Zhang, H. Fu, *Nano Res.* **2015**, *8*, 2998.
- [25] M. Johansen, C. Schlueter, P. L. Tam, L. E. Asp, F. Liu, *Carbon* **2021**, *179*, 20.
- [26] K. B. M. Ismail, M. A. Kumar, S. Mahalingam, B. Raj, J. Kim, *J. Energy Storage* **2024**, *84*, 110931.
- [27] F. N. Cogswell, *Thermoplastic Aromatic Polymer Composites*, Elsevier, Oxford **2013**, p. 214.
- [28] A. U. Sudhin, M. Remanan, G. Ajeesh, K. Jayanarayanan, *Mater. Today: Proc.* **2020**, *24*, 453.
- [29] A. Sayam, A. N. M. M. Rahman, M. S. Rahman, S. A. Smriti, F. Ahmed, M. F. Rabbi, M. Hossain, M. O. Faruque, *Carbon Lett.* **2022**, *32*, 1173.
- [30] D. Choi, H.-S. Kil, S. Lee, *Carbon* **2019**, *142*, 610.
- [31] P. R. Barnett, H. K. Ghossein, *Textiles* **2021**, *1*, 433.
- [32] Z. Liu, T. A. Turner, K. H. Wong, S. J. Pickering, *J. Cleaner Prod.* **2021**, *278*, 123785.
- [33] B. Newman, B. Dharmasiri, F. Stojcevski, K. A. S. Usman, S. A. Qin, J. M. Razal, L. C. Henderson, *Composites, Part A.* **2023**, *173*, 107658.
- [34] M. Kim, B. Goh, J. Kim, K.-S. Kim, J. Choi, *iScience* **2022**, *25*, 105367.
- [35] T. A. Khan, H. Kim, H.-J. Kim, *Failure Analysis in Biocomposites, Fibre-Reinforced Composites and Hybrid Composites*, Woodhead Publishing, Sawston **2019**, pp. 1–28.
- [36] E. Peled, C. Menachem, D. Bar-Tow, A. Melman, *J. Electrochem. Soc.* **1996**, *143*, L4.
- [37] M. Feng, S. Wang, Y. Yu, Q. Feng, J. Yang, B. Zhang, *Appl. Surf. Sci.* **2017**, *392*, 27.
- [38] T. Jin, G. Singer, K. Liang, Y. Yang, *Mater. Today.* **2023**, *62*, 151.
- [39] K. Moyer, N. A. Boucherbil, M. Zohair, J. Eaves-Rathert, C. L. Pint, *Sustainable Energy Fuels.* **2020**, *4*, 2661.
- [40] J. Xu, W. Johannisson, M. Johansen, F. Liu, D. Zenkert, G. Lindbergh, L. E. Asp, *Compos. Sci. Technol.* **2020**, *188*, 107962.
- [41] K. M. Beggs, L. Servinis, T. R. Gengenbach, M. G. Huson, B. L. Fox, L. C. Henderson, *Compos. Sci. Technol.* **2015**, *118*, 31.
- [42] L. Servinis, K. M. Beggs, T. R. Gengenbach, E. H. Doeven, P. S. Francis, B. L. Fox, J. M. Pringle, C. Pozo-Gonzalo, T. R. Walsh, L. C. Henderson, *J. Mater. Chem. A.* **2017**, *5*, 11204.

- [43] D. J. Eyckens, F. Stojcevski, A. Hendlmeier, C. L. Arnold, J. D. Randall, M. D. Perus, L. Servinis, T. R. Gengenbach, B. Demir, T. R. Walsh, L. C. Henderson, *Chem. Eng. J.* **2018**, *353*, 373.
- [44] B. Demir, K. M. Beggs, B. L. Fox, L. Servinis, L. C. Henderson, T. R. Walsh, *Compos. Sci. Technol.* **2018**, *159*, 127.
- [45] L. Servinis, L. C. Henderson, L. M. Andrichetto, M. G. Huson, T. R. Gengenbach, B. L. Fox, *J. Mater. Chem. A* **2015**, *3*, 3360.
- [46] C. Combelles, M. Delamar, F. Kanoufi, J. Pinson, F. I. Podvorica, *Chem. Mater.* **2005**, *17*, 3968.
- [47] X. Zhang, Y. Huang, T. Wang, L. Liu, *Composites, Part A* **2007**, *38*, 936.
- [48] L. Servinis, K. M. Beggs, C. Scheffler, E. Wölfel, J. D. Randall, T. R. Gengenbach, B. Demir, T. R. Walsh, E. H. Doeven, P. S. Francis, L. C. Henderson, *Carbon* **2017**, *118*, 393.
- [49] C. R. Birk, E. McTurk, M. R. Roberts, P. G. Bruce, D. A. Howey, *J. Electrochem. Soc.* **2015**, *162*, A2271.
- [50] P. Liu, E. Sherman, A. Jacobsen, *J. Power Sources* **2009**, *189*, 646.
- [51] X. Xiang, K. Zhang, J. Chen, *Adv. Mater.* **2015**, *27*, 5343.
- [52] D. Alvira, D. Antorán, J. J. Manyà, *J. Energy Chem.* **2022**, *75*, 457.
- [53] J. Zhu, S. W. Park, H. I. Joh, H. C. Kim, S. Lee, *Carbon Lett.* **2013**, *14*, 94.
- [54] S. Y. Kim, K. Yang, B.-H. Kim, *Electrochim. Acta* **2014**, *137*, 781.
- [55] S. N. Chaudhuri, R. A. Chaudhuri, R. E. Benner, M. S. Penugonda, *Compos. Struct.* **2006**, *76*, 375.
- [56] F.-W. Yuan, H.-J. Yang, H.-Y. Tuan, *ACS Nano* **2012**, *6*, 9932.
- [57] M. Fernando, P. Coia, M. G. Moloney, B. Dharmasiri, D. J. Hayne, T. Harte, E. Austria, B. Akhavan, L. C. Henderson, *Composites, Part B* **2025**, *289*, 111959.
- [58] D. Chukov, S. Nematulloev, V. Torokhov, A. Stepashkin, G. Sherif, V. Tcherdyntsev, *Results Phys.* **2019**, *15*, 102634.
- [59] X. Ma, C. Yuan, X. Liu, *Materials* **2015**, *7*, 75.
- [60] T. R. Gengenbach, G. H. Major, M. R. Linford, C. D. Easton, *J. Vac. Sci. Technol. A* **2021**, *39*, 013204.
- [61] M. Desaege, M. J. Reis, A. M. Botelho do Rego, J. D. L. da Silva, I. Verpoest, *J. Mater. Sci.* **1996**, *31*, 6305.
- [62] C. A. Fuentes, L. Q. N. Tran, C. Dupont-Gillain, W. Vanderlinden, S. De Feyter, A. W. Van Vuure, I. Verpoest, *Colloids Surf. A* **2011**, *380*, 89.
- [63] M. Delamar, R. Hitmi, J. Pinson, J. M. Saveant, *J. Am. Chem. Soc.* **1992**, *114*, 5883.
- [64] E. Pakdel, S. Kashi, R. Varley, X. Wang, *Resour. Conserv. Recycl.* **2021**, *166*, 105340.
- [65] D. He, P. Compston, E. Morozov, M. Doolan, *Procedia CIRP.* **2022**, *105*, 637.
- [66] A. Lopez-Urionabarrenechea, N. Gastelu, E. Acha, B. M. Caballero, A. Orue, A. Jiménez-Suárez, S. G. Prolongo, I. de Marco, *J. Cleaner Prod.* **2020**, *273*, 123173.
- [67] B. Akhavan, K. Jarvis, P. Majewski, *RSC Adv.* **2015**, *5*, 12910.
- [68] B. Akhavan, K. Jarvis, P. Majewski, *Langmuir* **2014**, *30*, 1444.
- [69] J. Zhang, W. Cheng, R. Zhang, T. Zeng, Y. Lei, H. Zhao, D. Luo, *Int. J. Low-Carbon Technol.* **2022**, *17*, 1216.
- [70] Y.-W. Xu, B.-H. Zhang, G.-R. Li, S. Liu, X.-P. Gao, *ACS Appl. Energy Mater.* **2020**, *3*, 487.
- [71] M. H. Kjell, E. Jacques, D. Zenkert, M. Behm, G. Lindbergh, *J. Electrochem. Soc.* **2011**, *158*, A1455.
- [72] S. Yoon, J. H. Ryu, S. M. Oh, C. Lee, *J. Non-Cryst. Solids* **2009**, *355*, 913.
- [73] S. Ahn, Y. Kim, K. J. Kim, T. H. Kim, H. Lee, M. H. Kim, *J. Power Sources* **1999**, *81–82*, 896.
- [74] E. Peled, *J. Electrochem. Soc.* **1979**, *126*, 2047.
- [75] B. G. Kim, D. W. Kang, G. Park, S. H. Park, S.-M. Lee, J. W. Choi, *Chem. Eng. J.* **2021**, *422*, 130017.
- [76] Y. Liang, Y. Chen, X. Ke, Z. Zhang, W. Wu, G. Lin, Z. Zhou, Z. Shi, *J. Mater. Chem. A* **2020**, *8*, 18094.
- [77] Q. Zhuang, L. Tian, G. Wei, Q. Dong, S. Sun, *Chin. Sci. Bull.* **2009**, *54*, 2627.
- [78] M. Steinbauer, S. Risse, N. Wagner, K. A. Friedrich, *Electrochim. Acta* **2017**, *228*, 652.
- [79] H. Schranzhofer, J. Bugajski, H. J. Santner, C. Korepp, K. C. Möller, J. O. Besenhard, M. Winter, W. Sitte, *J. Power Sources* **2006**, *153*, 391.
- [80] X. Rao, Y. Lou, J. Zhao, J. Chen, Y. Qiu, T. Wu, S. Zhong, H. Wang, L. Wu, *J. Porous Mater.* **2023**, *30*, 403.

Manuscript received: June 18, 2025

Revised manuscript received: October 10, 2025

Version of record online: